Acta metall. mater. Vol. 41, No. 1, pp. 279–296, 1993
Printed in Great Britain.

0956-7151/93 $5.00 + 0.00

KINETICS OF STRAIN-INDUCED MORPHOLOGICAL TRANSFORMATION IN CUBIC ALLOYS WITH A MISCIBILITY GAP

Y. WANG, L.-Q. CHEN† and A. G. KHACHATURYAN

Department of Materials Science and Engineering, Rutgers University, P.O. Box 909, Piscataway, NJ 08855, U.S.A.

(Received 4 March 1992)

Abstract—Morphological evolutions controlled by a transformation-induced elastic strain during a solid state precipitation are systematically investigated using a prototype binary alloy as a model system. A computer simulation technique based on a microscopic kinetic model including the elastic strain effect is developed. Without any *a priori* assumptions concerning shapes, concentration profiles and mutual positions of new phase particles, various types of coherent two-phase morphologies such as basket-weave structures, sandwich-like multi-domain structures, precipitate macrolattices and GP zones are predicted. A wide variety of interesting strain-induced kinetic phenomena are observed during development of the above microstructures, including selective and anisotropic growth, reverse coarsening, particle translational motion, particle shape transition and splitting. In spite of all simplifications of the model, most of the simulation results are confirmed by experimental observations in various alloy systems, indicating that this kinetic model can be efficiently used for understanding, interpreting and predicting structural evolutions in real alloys.

Résumé—On étudie systématiquement les évolutions morphologiques contrôlées par une déformation élastique induite par transformation pendant une précipitation à l'état solide en utilisant un alliage binaire prototype comme système modèle. On développe une technique de simulation numérique basée sur un modèle cinétique microscopique incluant l'effet de déformation élastique. Sans aucune hypothèse *a priori* concernant les formes, on prévoit les profils de concentration et les positions mutuelles des particules des nouvelles phases, les différents types de morphologies des mélanges biphasés cohérents tels que les structures tissées en panier, les structures à plusieurs domaines en sandwich, les macroréseaux précipités et les zones de G.P. On observe une grande variété de phénomènes cinétiques intéressants induits par la déformation pendant le développement des microstructures ci-dessus, y compris une croissance sélective et anisotrope, un grossissement inversé, un mouvement de translation des particules, une transition de forme et une scission des particules. Malgré toutes les simplifications du modèle, la plupart des résultats des simulations sont confirmés par les observation expérimentales dans divers systèmes d'alliages, ce qui indique que ce modèle cinétique peut être utilisé efficacement pour comprendre, interpréter et prévoir les evolutions structurales dans les alliages réels.

Zusammenfassung—An einem Modellsystem einer binären Prototyplegierung werden die morphologischen Entwicklungen, wie sie von umwandlungsinduzierten, durch Ausscheidungsprozesse hervorgerufenen elastischen Verzerrungen im Festkörper gesteuert werden, systematisch untersucht. Hierzu wird ein Simulationsverfahren entwickelt, welches auf einem kinetischen Modell beruht, welches Effekte durch die elastischen Verzerrungen einschließt. Ohne Annahmen über Gestalt, Konzentrationsprofile und gegenseitige Lage der neuen Phasenteilchen zu machen, werden verschiedene kohärente zweiphasige Morphologien, wie Korbgewebe-Struktur, schichtartige Vieldomänen-Strukturen, Ausscheidungs-Makrogitter und Guinier-Preston-Zonen, vorausgesagt. Eine große Vielfalt interessanter dehnungsinduzierter kinetischer Erscheinungen wird während der Entwicklung dieser Mikrostrukturen beobachtet, dazu gehören selektives und anisotropes Wachstum, umgekehrte Vergröberung, Translationsbewegung der Teilchen, Umwandlung und Aufspalten der Teilchengestalt. Trotz aller Vereinfachungen des Modelles werden die meisten Simulationsergebnisse, durch experimentelle Beobachtungen in verschiedenen Legierungssystemen bestätigt. Mit diesem Modell können also die strukturellen Entwicklungen in wirklichen Legierungen verstanden, interpretiert und vorausgesagt werden.

1. INTRODUCTION

Solid state precipitation is one of the most efficient ways to develop desirable microstructures for advanced engineering materials, such as nickel based high-temperature superalloys and aluminum and magnesium based ultralight alloys. The thermodynamic driving forces for precipitation result in an extensive atomic rearrangement towards a stable equilibrium corresponding to a minimum in free energy. Depending on the transformation kinetics, however, a series of intermediate metastable and transient morphological states of a mixture of precipitate and matrix phases can be formed in the

†Permanent address: Department of Materials Science and Engineering, Pennsylvania State University, University Park, PA 16802, U.S.A.

path to equilibrium. Study of the structural transformations along this path continues to be a subject of wide interest in materials science.

The kinetics of morphological evolution depends strongly on the thermodynamic driving force. If there are no external fields (such as stress or magnetic), the driving forces for precipitation are reductions of bulk free energy, interfacial energy and transformation-induced strain energy. According to classical thermodynamics, the bulk free energy determines compositions and volume fractions of equilibrium phases in a two-phase mixture. Unlike the bulk free energy, the interfacial energy depends on a two-phase morphology. As for the transformation-induced strain energy, it has an unconventional dependence on both the volume and morphology of the product phases. Being volume-dependent, the strain energy contributes to the equilibrium compositions and volume fractions of the coexisting phases, whereas being morphology-dependent, it also affects the mesoscale alloy microstructure.

According to the classical Lifshitz–Slyozov–Wagner (LSW) theory, if the interfacial energy is the only driving force, the linear dimension of any microstructural feature of a new phase particle increases in time following a simple dynamic scaling law. It leaves the equilibrium shapes and mutual arrangement of new phase particles unaltered. The situation is, however, significantly different if the microstructural changes are controlled by an accommodation of the transformation-induced elastic strain. It is well known that if the atomic rearrangement in a precipitate reaction gives rise to a new phase whose crystal lattice parameter differs from that of its parent phase and is coherently embedded in it, elastic strain fields are generated around the new phase particles. Overlap of these strain fields results in a strain-induced interaction between finite elements of the product phases. Being strongly orientation dependent and having an infinite radius of interaction decaying as $1/r^3$, the strain-induced interaction is similar to the magnetic or electric dipole–dipole interactions. Accordingly, the strain energy is strongly dependent on sizes, shapes, orientations and mutual arrangements of precipitate particles [1]. In such a case, complicated morphological changes are expected. The TEM and X-ray studies of many technologically important alloy systems have demonstrated that this is exactly the case. Various types of elaborate coherent two-phase morphologies (such as precipitate macrolattice in Fe–Be [2, 3] and basket-weave structures in ALNICO [4] and β-brass [5]) as well as different kinds of strain-induced kinetic phenomena (such as particle shape transition and splitting [6, 7] and strong precipitate correlations [8–10]) were observed.

Theoretical study of the elastic strain effects on a multi-particle morphology of two-phase systems originated from the classical work by Cahn [11] who studied an early stage isostructural spinodal decomposition in a cubic alloy. He solved the linearized diffusion equation with a strain energy contribution and first demonstrated that spinodal decomposition in an elastically anisotropic system occurs by developing concentration waves along the elastically soft directions. These concentration waves lead to satellites near the Bragg reflections along the soft directions in reciprocal space.

A close equation describing the strain energy of a two-phase mixture of an arbitrary morphology was derived by Khachaturyan [12] and Khachaturyan and Shatalov [13]. They showed that a strain accommodation leads to a development of certain optimal microstructures. So far, the equilibrium shape and habit of a single coherent new phase particle in an anisotropic crystal [1, 12, 14] and the mutual arrangements of a group of precipitates (e.g. the so-called modulated structures [1, 15–18] and the tweed and twin structures [19]) were predicted by minimizing the strain energy. Although these thermodynamic approaches could explain origins of some strain-induced morphologies, they cannot account for details of the morphological evolution along the transformation path. Since the most interesting morphologies almost always appear at intermediate stages of a phase transformation, this is a substantial disadvantage.

The linear diffusion theory by Cahn gives certain important information on the initial stages of spinodal decomposition. However, when the local compositions become close to the equilibrium values, further decomposition of a system is controlled by nonlinear effects. It is coarsening, particularly strain-induced coarsening that determines the morphological evolution of a two-phase mixture after the short initial linear stage. Extension of the linear approach to the nonlinear stage of spinodal decomposition has been proposed by Miyazaki *et al.* [20]. These authors obtained numerical solution of the nonlinear Cahn–Hilliard equation. Kinetics of a strain-induced coarsening starting from randomly distributed elementary particles (finite elements) of the precipitate phase has been investigated by Wen *et al.* [21]. By assuming that the morphological changes occur along the steepest total free energy descent path (strain energy + interfacial energy), evolutions of the randomly distributed precipitates into modulated structures and tweed structures were predicted by a computer simulation. McCormack *et al.* [22] analyzed the kinetics of particle splitting phenomenon using the same technique. However, this approach cannot describe the early stage decomposition where the concentration waves first develop. Evolution of concentration profiles during the coarsening was also ignored. These aspects may have a profound influence on the later stage coarsening.

The effect of strain on the Ostwald ripening kinetics of two spherical particles in an infinite anisotropic crystal was recently examined by Johnson *et al.* [23] who used an analytical approach. In this approach, shapes of the particles are assumed

unchanged during the whole coarsening process. However, a spherical shape of a particle can be expected only if an isotropic interfacial energy rather than strain energy dominates the coarsening process (this may be the case in the initial stage of coarsening). When the particles grow above a certain critical size, the strain energy dominates over the interfacial energy and the particles are no longer spherical. Some preliminary results, free from any of these limitations, have been obtained in our computer simulations [24].

It is the purpose of this paper to investigate the effects of coherent elastic strains on the kinetics of morphological transformations in solid state precipitations without any *a priori* assumptions on the possible morphologies that could develop. To reach such an objective, a kinetic model based on the microscopic diffusion theory [25] and microscopic elasticity theory of an arbitrary solid solution [1, 12, 13] is constructed. In this model, all structural changes, both atomic and mesoscale, are described in terms of a single-site occupation probability function of finding a solute atom at a crystal lattice site. The problems of morphological transformation are then reduced to a temporal evolution of this function. This approach is actually universal in a sense that it can simultaneously describe a wide variety of very different structural transformations, such as ordering, decomposition, growth and coarsening, within the same formalism. The diffusional relaxation of this function towards its equilibrium state is described by the Önsager-type microscopic diffusion equations [25]. Because the driving force of the crystal lattice diffusion process is a highly nonlinear functional of the occupation probability function, the diffusion equations are strongly nonlinear and can only be solved numerically by using computer simulation techniques. The reciprocal space formulation of the microscopic diffusion theory and the microscopic elasticity theory allows a straightforward computer simulation. The advantages of such a kinetic model has been demonstrated in the study of precipitation of an ordered intermetallic phase from a disordered solid solution without elastic strain [26, 27]. To focus on the coherent elastic strain effect, however, we shall only consider a simple case in this paper, i.e. an isostructural decomposition of a cubic disordered phase into a mixture of two cubic disordered phases in a binary alloy.

The results may also be applied to a more complicated case when the precipitate phase is an ordered intermetallic. It has been shown [26, 27] that precipitation of an ordered intermetallic from a disordered matrix is preceded by a congruent ordering, which results in an ordered single-phase forming a nanoscale mixture of antiphase domains. The decomposition is heterogeneous. It is dominated by an antiphase domain boundary (APB) instability which leads to the replacement of APBs by the equilibrium disordered phase. The situation, however, changes if a stable high-temperature ordered phase rather than the disordered state is quenched into the two-phase field. The initial high-temperature ordered phase may consist of large ordered domains and thus the spinodal decomposition may occur homogeneously within the bulk of the initial ordered phase. This decomposition is isostructural and is controlled by a conditional spinodal suggested by Allen and Cahn [28]. An example is the isostructural decomposition of an ordered phase occurred in ALNICO alloys. In such cases the morphological evolution should not be different from that predicted in this paper. Some effects of transformation-induced elastic strain on precipitation of an ordered intermetallic from a disordered matrix has recently been studied [29].

2. THEORETICAL BASIS

2.1. Formulation of the kinetic model

According to [25], the crystal lattice site diffusion in a binary substitutional alloy is determined by a diffusional relaxation of the nonequilibrium single-site occupation probability of finding a solute atom at crystal lattice site, $\mathbf{r}$, and at time, t, which is given by $n(\mathbf{r}, t)$. The diffusional relaxation is described by the Önsager equation

$$\frac{\mathrm{d}n(\mathbf{r}, t)}{\mathrm{d}t} = \frac{c(1-c)}{k_B T} \sum_{\mathbf{r}'} L_0(\mathbf{r}-\mathbf{r}') \frac{\delta F}{\delta n(\mathbf{r}', t)} \tag{1}$$

where c is the atomic fraction of solute atoms, k_B is the Boltzmann's constant, T is the absolute temperature, $L_0(\mathbf{r}-\mathbf{r}')$ is a matrix of kinetic coefficients related to probabilities of elementary diffusional jumps from lattice site $\mathbf{r}$ to $\mathbf{r}'$ of a Bravais lattice during a time unit, and F is the total free energy including the strain energy contribution. The summation over $\mathbf{r}'$ is carried out over all N lattice sites of a crystal. The conservation of atoms in the system gives a relation

$$\sum_{\mathbf{r}} L_0(\mathbf{r}-\mathbf{r}') = 0.$$

In the case of an ideal solid solution, equation (1) describes a random walk problem. In the long-wave approximation, equation (1) gives the conventional Cahn–Hilliard equation. The solution of equation (1) is substantially simplified if the Fourier transform technique is used. The Fourier representation of equation (1) reads

$$\frac{\mathrm{d}\tilde{n}(\mathbf{k}, t)}{\mathrm{d}t} = \frac{c(1-c)}{k_B T} \tilde{L}_0(\mathbf{k}) \left\{ \frac{\delta F}{\delta n(\mathbf{r}, t)} \right\}_{\mathbf{k}} \tag{2}$$

where $\mathbf{k}$ is the reciprocal lattice vector, and $\tilde{n}(\mathbf{k}, t)$, $\tilde{L}_0(\mathbf{k})$, and $\{\delta F/\delta n(\mathbf{r}, t)\}_{\mathbf{k}}$ are Fourier transforms of the corresponding real space functions.

2.2. The free energy approximation

To describe the free energy entering equation (1), we utilize the mean-field approximation. In the

mean-field approximation, the free energy for an inhomogeneous solid solution is given by

$$F = \tfrac{1}{2}\sum_{\mathbf{rr}'} W(\mathbf{r}-\mathbf{r}')n(\mathbf{r})n(\mathbf{r}') + k_B T \sum_{\mathbf{r}} [n(\mathbf{r})\ln n(\mathbf{r}) + (1-n(\mathbf{r}))\ln(1-n(\mathbf{r}))] \quad (3)$$

where $W(\mathbf{r}-\mathbf{r}') = w(\mathbf{r}-\mathbf{r}')_f + w(\mathbf{r}-\mathbf{r}')_{el}$ is a pairwise interaction energy between two atoms at lattice sites $\mathbf{r}$ and $\mathbf{r}'$, including a finite radius ("chemical") interaction $w(\mathbf{r}-\mathbf{r}')_f$ and an infinite radius strain-induced interaction $w(\mathbf{r}-\mathbf{r}')_{el}$. Since the focus of this paper is on the main characteristics of a two-phase morphological evolution during a precipitation reaction, any free energy approximation which provides a convex segment on the free energy vs composition curve corresponding to a miscibility gap can be used. The mean-ffeld approximation seems to be the simplest model to work with. It should be noted that differences between various free energy models with convex segments on their free energy vs composition curve would not affect the sequence of transient structures along the transformation path that we are primarily interested in. It may only affect the rate of transformation. The bulk free energy, interfacial energy and strain energy used in the phenomenological Cahn–Hilliard model are automatically described by equation (3). For example, they can be obtained by a limit transition of (3) to the continuum theory [1].

2.3. Elastic strain energy

In the microscopic elasticity theory [1, 12, 13], the strain energy of a binary solid solution is given as a sum of two physically distinct terms: (i) the configuration-independent term describing the self-energy and image force-induced energy, (ii) the configuration-dependent term associated with concentration inhomogeneity. The first term is not affected by spatial redistribution of solute atoms and therefore it can be ignored. The second term however gives a substantially nonlocal strain energy change associated with spatial distribution of solute atoms. Since such a strain energy also depends on the volume of the precipitate phase, it plays a key role in structural transformations. Therefore, we shall concentrate on only this part of the strain energy in this study.

For a cubic substitutional solid solution, solute atoms are dilatational centers and their introduction leads to an isotropic crystal lattice expansion characterized by a stress-free strain tensor $\epsilon^0_{ij} = \epsilon_0 \delta_{ij}$, where $\epsilon_0 = \mathrm{d}a/a\ \mathrm{d}c$ is the concentration coefficient of crystal lattice expansion caused by the atomic size difference, a is the crystal lattice parameter of a solid solution, c is the atomic fraction of solute atoms and δ_{ij} is the Kronecker delta symbol. Under these conditions, the configuration-dependent strain energy associated with an arbitrary atomic distribution, $n(\mathbf{r})$, is [1]

$$E_{el} = \frac{1}{2N}\sum_{\mathbf{k}}{}' V(\mathbf{k})_{el}|\tilde{n}(\mathbf{k})|^2 \quad (4)$$

where $V(\mathbf{k})_{el}$ is the Fourier transform of the infinite radius strain-induced interaction energy, $w(\mathbf{r})_{el}$, and $\tilde{n}(\mathbf{k})$ is the Fourier transform of $n(\mathbf{r})$. The prime in the summation (4) implies that the point $\mathbf{k}=0$ is excluded.

Since a decomposition process is determined by development of a packet of concentration waves with wave vectors close to zero, the long-wave (continuum) approximation for $V(\mathbf{k})_{el}$ [1] can be used

$$V(\mathbf{k})_{el} \approx B(\mathbf{e}) = -\sigma_0^2[e_i\Omega(\mathbf{e})_{ij}e_j - \langle e_i\Omega(\mathbf{e})_{ij}e_j\rangle_e] \quad (5)$$

where $\sigma_0 = (c_{11}+2c_{12})\epsilon_0$, c_{11} and c_{12} are elastic constants of a cubic crystal, $\mathbf{e} = \mathbf{k}/k$ is a unit vector in the $\mathbf{k}$ direction, $\Omega(\mathbf{e})_{ij}$ is a Green tensor reciprocal to $C_{ijkl}e_k e_l$ (C_{ijkl} is a tensor of the elastic constants) and $\langle\cdots\rangle_e$ is a symbol of averaging over all directions $\mathbf{e}$. In (5), the Einstein suffix notation is used. At $\mathbf{k}=0$, the function $B(\mathbf{e})$ has a singularity since its limit at $\mathbf{k}\to 0$ depends on the $\mathbf{k}$ vector direction. This singularity results in a long-range asymptotic behavior of the strain-induced interaction in real space [13]. Rewriting equation (4) in a real space representation gives

$$E_{el} = \tfrac{1}{2}\sum_{\mathbf{rr}'} w_{el}(\mathbf{r}-\mathbf{r}')n(\mathbf{r})n(\mathbf{r}'). \quad (6)$$

The Fourier transform of the variational derivative of (3) yields

$$\left\{\frac{\delta F}{\delta n(\mathbf{r},t)}\right\}_{\mathbf{k}} = V(\mathbf{k})n(\mathbf{k},t) + k_B T\left\{\ln\frac{n(\mathbf{r},t)}{1-n(\mathbf{r},t)}\right\}_{\mathbf{k}} \quad (7)$$

where

$$V(\mathbf{k}) = \sum_{\mathbf{r}}[w(\mathbf{r})_f + w(\mathbf{r})_{el}]\exp(-i\mathbf{kr}) = V(\mathbf{k})_f + B(\mathbf{e}) \quad (8a)$$

$$V(\mathbf{k})_f = \sum_{\mathbf{r}} w(\mathbf{r})_f \exp(-i\mathbf{kr}) \quad (8b)$$

$$\left\{\ln\left(\frac{n(\mathbf{r},t)}{1-n(\mathbf{r},t)}\right)\right\}_{\mathbf{k}} = \sum_{\mathbf{r}}\ln\left(\frac{n(\mathbf{r},t)}{1-n(\mathbf{r},t)}\right)\exp(-i\mathbf{kr}). \quad (8c)$$

Substituting (8) to (7) and (7) to (2) yields a reciprocal space representation of the kinetic equation

$$\frac{\mathrm{d}\tilde{n}(\mathbf{k},t)}{\mathrm{d}t} = \frac{c(1-c)}{k_B T}\tilde{L}_0(\mathbf{k})\left[(V(\mathbf{k})_f + B(\mathbf{e}))\tilde{n}(\mathbf{k},t) + k_B T\left\{\ln\frac{n(\mathbf{r},t)}{1-n(\mathbf{r},t)}\right\}_{\mathbf{k}}\right]. \quad (9)$$

The mean field approximation which results in equation (9) is good for any system with long-range interactions. The longer the interaction range, the more accurate the equation. It is especially accurate in the presence of long-range strain-induced interactions [30]. Due to the nonlinear term in the square bracket, equation (9) is a nonlinear equation with respect to $\tilde{n}(\mathbf{k},t)$. It is obvious that a numerical solution would be preferred for dealing with any problems of practical significance.

The significant advantage of equation (9) for the study of morphological transformation is that the only input needed is the information concerning interaction potentials. They are the finite radius and strain-induced infinite radius interactions described in the reciprocal space by functions $V(\mathbf{k})_f$ and $B(\mathbf{e})$, respectively. A solution of it, $\tilde{n}(\mathbf{k}, t)$, completely describes the temporal and spatial evolution of the concentration wave amplitudes within the entire first Brillouin zone. The back Fourier transform of the function, $\tilde{n}(\mathbf{k}, t)$, gives the occupation probabilities, $n(\mathbf{r}, t)$, which describe both the atomic scale and mesoscale microstructure transformations, including changes of crystal structures, shapes, habits, concentration profiles and mutual distributions of the precipitates. Any *a priori* assumptions concerning the above information become unnecessary.

3. MODEL SYSTEMS

In the present work we consider 2D binary substitutional solid solution of an isostructural decomposition in a square lattice consisting of 128 × 128 unit cells. Periodic boundary conditions are applied along both dimensions. This is the simplest model approximating the main features of morphological transformation in a cubic system. We assume that the two disordered product phases have the same disordered structure and elastic moduli, but different compositions and thus different crystal lattice parameters. A coherency between the precipitate and matrix phases is assumed. The interaction energies of the system are chosen in such a way that they lead to an isostructural decomposition when the system is quenched to a lower temperature. This means that the function $V(\mathbf{k})_f$ in (9) assumes its minimum value at $\mathbf{k} = 0$.

Since $V(\mathbf{k})_f$ describes the finite radius atomic interaction, its back Fourier transform, the interchange energies $w(\mathbf{r})_f$, have nonvanishing values only for a few coordination shells. Therefore we assume a 2-neighbor interaction model in this study (interactions beyond the second coordination shell are assumed to be zero). The function $V(\mathbf{k})_f$ in this 2D model could be written as

$$V(\mathbf{k})_f = 2w_1(\cos k_x a + \cos k_y a) + 4w_2 \cos k_x a \cos k_y a \tag{10}$$

where $\mathbf{k} = (k_x, k_y)$, k_x and k_y are components of the vector $\mathbf{k}$ along the x and y axes parallel to the [10] and [01] directions in the reciprocal space, w_1 and w_2 are the nearest and next nearest neighbor pairwise interchange energies and a is the crystal lattice parameter. Both w_1 and w_2 are assumed negative and w_1/w_2 ratio is chosen to be $\sqrt{2}$. This particular choice of w_1 and w_2 results in a miscibility gap in the phase diagram and provides equal interfacial energies of {10} and {11} interfaces. The condition of equal interfacial energies of the {10} and {01} interfaces allows us to simulate a nearly isotropic interfacial energy within the assumed 2-neighbor interaction model and thus, to exclude all anisotropic effects other than those caused by the elastic strain.

The infinite radius strain-induced interaction described by equation (5) for this 2D model can be well approximated as

$$B(\mathbf{e}) \approx B(e_x^2 e_y^2 - \tfrac{1}{8}) \tag{11}$$

where e_x and e_y are components of the unit vector $\mathbf{e}$ along the x and y axes in the reciprocal space and

$$B = -\frac{4(c_{11} + 2c_{12})^2}{c_{11}(c_{11} + c_{12} + 2c_{44})} \epsilon_0^2 \Delta \tag{12}$$

is a material constant. It characterizes the elastic properties and the crystal lattice mismatch and is defined as strain energy parameter in this paper. In (12), $\Delta = c_{11} - c_{12} - 2c_{44}$ is the elastic anisotropy constant and c_{11}, c_{12}, c_{44} are elastic contants of the model system. In our simulation $B > 0$ which occurs for alloys with a negative elastic anisotropy. The term 1/8 in (11) is $\langle e_x^2 e_y^2 \rangle$.

Since the interatomic interaction chosen provides decomposition, the phase diagram can be determined simply by minimizing the free energy

$$F = N[\tfrac{1}{2} V(0) c^2 + k_B T(c \ln c + (1 - c) \ln(1 - c))] \tag{13}$$

which follows equation (3) with $n(\mathbf{r}) \to c$ [1]. However, due to involvement of the infinite radius strain-induced interaction characterized by the function $B(\mathbf{e})$ which has a singularity at $\mathbf{k} = 0$, the situation is complicated. Instead of $V(0)$, we have to use $\min[V(\mathbf{k})] = V(0)_f + B(\mathbf{e}_0)$, where $\mathbf{e}_0 = \langle 01 \rangle$ is the "soft" directions providing the minimum value of $B(\mathbf{e})$ [according to (11), $B(\mathbf{e}_0) = -B/8$]. It should be noted that the singularity of $V(\mathbf{k}) = V(\mathbf{k})_f + B(\mathbf{e})$ at $\mathbf{k} = 0$ is responsible for the dependence of the bulk free energy on the two-phase morphology, leading to a very unconventional situation where the mesoscale morphology (shape, habit and spatial arrangement of the second phase particles) determines the phase identity. In other words, different morphologies can be regarded as different phases. The stable coherent diagram calculated from the free energy model

$$F = N\left[\tfrac{1}{2}\left(V(0)_f - \frac{B}{8}\right)c^2 + k_B T(c \ln c + (1 - c) \ln(1 - c))\right] \tag{14}$$

is shown in Fig. 1, which corresponds to infinite thin precipitates normal to $\mathbf{e}_0 = \langle 01 \rangle$. All other morphologies correspond to metastable states whose miscibility gaps are inside the one presented in Fig. 1. The diagram is presented in terms of a reduced temperature $T^* = k_B T / |V(0)_f - B/8|$.

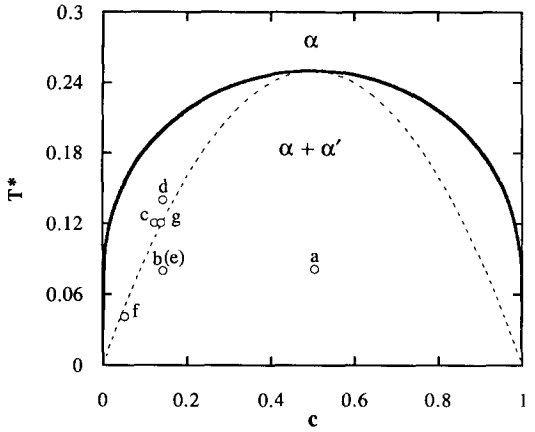

Fig. 1. Coherent equilibrium phase diagram for plate-like precipitates of {01} habits of the model system. The miscibility gap is designated by a solid line and the dashed line describes the spinodal. The diagram is presented in terms of a reduced temperature T^* (see text for the definition of T^*). Open circles marked a–g represent the alloy compositions and "aging" temperatures chosen for the computer simulations.

By assuming that the elementary diffusional jumps occur only among the nearest and next nearest neighbor sites and utilizing the relation

$$\sum_{\mathbf{r}} L_0(\mathbf{r}) = 0,$$

the function $\tilde{L}_0(\mathbf{k})$ in (9) for this 2D model may be expressed as follows

$$\begin{aligned}\tilde{L}(\mathbf{k})_0 &= \sum_{\mathbf{r}} L_0(\mathbf{r})\exp(-i\mathbf{kr}) \\ &= -2L_1[(2-\cos k_x a-\cos k_y a) \\ &\quad +\alpha(2-\cos(k_x a+k_y a) \\ &\quad -\cos(k_x a-k_y a))] \qquad (15)\end{aligned}$$

where $\alpha = L_2/L_1$, L_1 and L_2 are kinetic coefficients of elementary diffusional jumps to the nearest and next nearest neighbor sites, respectively. In this study L_1 and L_2 are assumed to be independent of alloy composition. This conventional approximation for atomic mobilities in diffusion kinetics may affect the transformation rate but not a sequence of the structural evolutions. The value of α is assumed to be 0.1. The purpose of using such a 2-neighbor jump model instead of the nearest-neighbor jump model is to accelerate the numerical calculations. The features and sequences of the simulated morphological evolution do not depend on α. Using (10)–(12) and (15) in (9) and introducing the reduced strain energy parameter, $B^* = B/|V(0)-B/8|$, and reduced time $t^* = t/\tau$, where $\tau = [L_1(c(1-c)/k_B T)|V(0)-B/8|]^{-1}$ is a typical time of an elementary diffusion event, the kinetic equation (9) for this 2D model system may be written in a dimensionless form

$$\begin{aligned}\frac{\mathrm{d}\tilde{n}(\mathbf{k},t^*)}{\mathrm{d}t^*} &= -2[(2-\cos k_x a-\cos k_y a) \\ &\quad +\alpha(2-\cos(k_x a+k_y a) \\ &\quad -\cos(k_x a-k_y a))] \\ &\quad \times\left[\frac{2w_1}{|V(0)-B/8|}(\cos k_x a+\cos k_y a)\right. \\ &\quad +\frac{4w_1/\sqrt{2}}{|V(0)-B/8|}\cos k_x a\cos k_y a \\ &\quad +B^*(e_x^2 e_y^2-\tfrac{1}{8})\tilde{n}(\mathbf{k},t^*) \\ &\quad \left.+T^*\left\{\ln\frac{n(\mathbf{r},t^*)}{1-n(\mathbf{r},t^*)}\right\}_{\mathbf{k}}\right]. \qquad (16)\end{aligned}$$

Solution of this equation is carried out using the Euler method relating occupation probabilities at the time moments t^* and $t^*+\Delta t^*$ by a recurrence equation

$$\tilde{n}(\mathbf{k},t^*+\Delta t^*) = \tilde{n}(\mathbf{k},t^*)+\frac{\mathrm{d}\tilde{n}(\mathbf{k},t^*)}{\mathrm{d}t^*}\Delta t^* \qquad (17)$$

where Δt^* is a time increment and $\mathrm{d}\tilde{n}(\mathbf{k},t^*)/\mathrm{d}t^*$ is expressed in terms of $\tilde{n}(\mathbf{k},t^*)$ through equation (16).

4. SIMULATION RESULTS

4.1. Morphological evolution during spinodal decomposition

Spinodal decompositions are simulated by isothermally "aging" the homogeneous disordered solid solutions below the spinodal line of the phase diagram shown in Fig. 1. The as-quenched state of the system is determined by an initial condition $n(\mathbf{r},0) = c+\delta c(\mathbf{r})$, where c is the average composition of the solution and $\delta c(\mathbf{r})$ are small perturbations generated by a random number generator. Typical spatial and temporal evolutions of the as-quenched microstructures are presented in Figs 2 and 3. In these figures and the following ones, completely dark regions in the simulated microstructures represent a zero occupation probability, $n(\mathbf{r},t^*)$, for solute atoms, while completely white regions describe an occupation probability of one. All the intermediate values of $n(\mathbf{r},t^*)$ are represented by different shades of grey. Small dark squares in the lower right corners of each piccture in Fig. 2 and the following figures are simulated diffraction patterns around $\mathbf{k}=0$, described by $|\tilde{n}(\mathbf{k},t^*)|^2$. In order to give a better image, the Bragg reflection intensity is removed from the diffraction pattern and only diffuse scattering due to concentration heterogeneities is shown. The intensities of satellites are normalized to their maximum values for each pattern.

4.1.1. Spinodal decomposition in a symmetrical case. An alloy with composition $c=0.5$ is aged at a temperature, $T^*=0.08$. The corresponding point in the phase diagram is shown in Fig. 1 by point "a", which sits right in the middle of the miscibility gap.

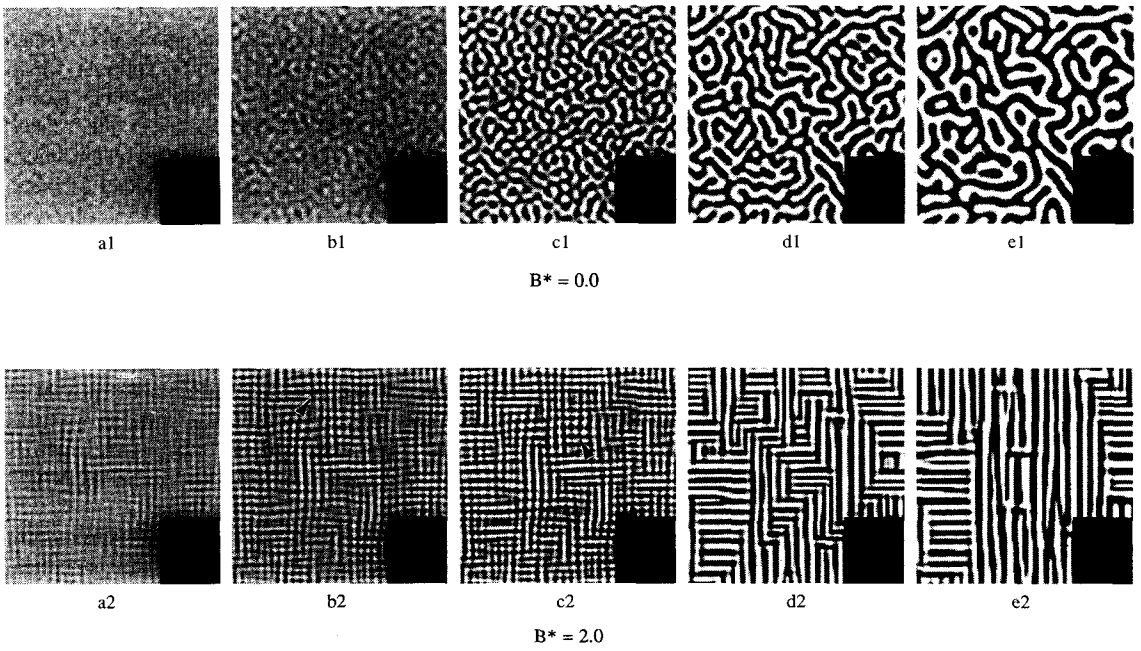

Fig. 2. Simulated temporal isothermal evolutions of microstructures in alloys undergoing symmetrical spinodal decomposition at point "a" in Fig. 1. Various shades of grey represent different values of occupation probability of solute atoms (completely white represents a value of one while completely dark represents a value of zero). The insets represent normalized diffuse scattering intensities around reciprocal lattice origin. (a1)–(e1) correspond to reduced transformation time t^* (see text for definition) = 8, 10, 15, 30, 50, and (a2)–(e2) correspond to $t^* = 4, 5, 6, 20, 50$. 1 and 2 refer to two different cases where the reduced strain energy parameter B^* equals to 0.0 and 2.0, respectively.

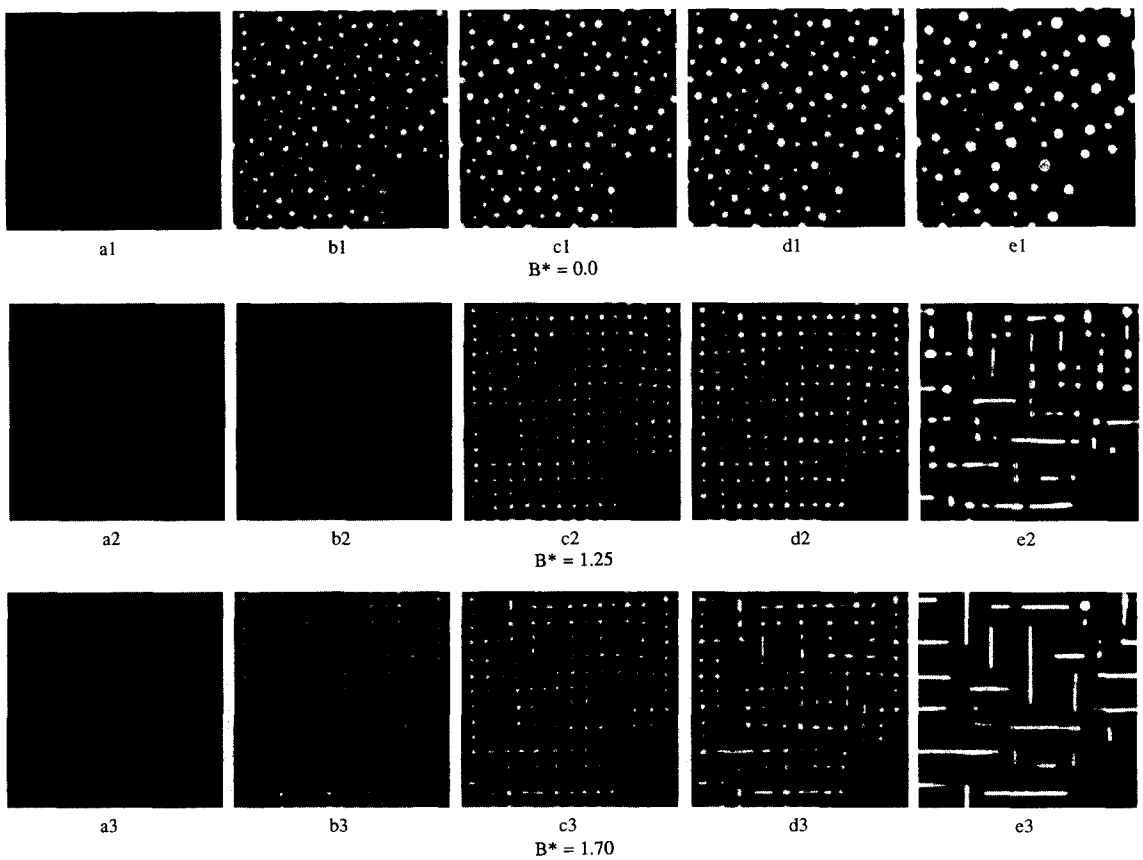

Fig. 3. Temporal morphological evolutions in alloys undergoing asymmetrical spinodal decomposition at point "b" in Fig. 1, (a1)–(e1), (a2)–(e2) and (a3)–(e3) correspond to $t^* = 40, 60, 80, 100$ and 180. 1, 2 and 3 refer to three different cases where the reduced strain energy parameter B^* equals to 0.0, 1.25 and 1.70, respectively.

Several simulations with different values of B^* have been performed. Two typical results with $B^* = 0.0$ and $B^* = 2.0$ are presented in Fig. 2. The finite radius interchange energies, w_1 and w_2 are kept the same in both cases. Therefore a change in B^* actually means a change in the balance between the strain-induced infinite radius interaction and the finite radius "chemical" interaction. Starting from the same initial morphology of a homogeneous state, which is not shown in the figures, the computer simulations show gradual transformations of the two alloys into totally different spatial patterns of a mixture of the two equilibrium phases. Let us first consider decomposition in an extreme case of $B^* = 0.0$, i.e. no strain energy contribution is included. As shown in Fig. 2 (a1–e1), the spinodal decomposition starts by developing concentration waves along all directions. The corresponding side-bands shown in the diffraction patterns form rings. The amplitudes of these concentration waves keep growing until the occupation probabilities reach values equal to equilibrium compositions. The growth stage then comes to an end and the system starts to coarsen. There is a considerable increase in the wave length at this stage [see, e.g. Fig. 2(c1–e1)], which is clearly indicated by the shrinkage of the side band rings in the diffraction patterns. However, the general features of the morphology do not change during the entire coarsening process. For example, the two product phases maintain to be highly interconnected and randomly oriented. This kind of morphology is quite similar to that predicted by Cahn [31] using a simple linearized theory of spinodal decomposition in elastically isotropic systems, and is reminiscent of those observed in many experimental studies of phase separations in isotropic systems such as glasses.

When a significant lattice mismatch between the two product phases is assumed, e.g. $B^* = 2.0$, a highly anisotropic structure composed of alternative $\{01\}$ thin strips of the two product phases is obtained [Fig. 2(a2–e2)]. In the early stage of decomposition, only concentration waves along the elastically soft directions (i.e. [10] and [01]) develop. The side-band formed in the diffraction pattern in this case consists of only satellites along the $\langle 01 \rangle$ directions. Superposition of these waves while they grow towards their equilibrium amplitudes generates an interesting intermediate structure which looks like a "basket weave" (see a2–c2 in Fig. 2). It consists of solute-rich white strips and solute-lean dark strips weaving together along the soft directions. This morphology is in striking agreement with experimental observations by de Vos in ALNICO alloy [4], Butler and Thomas [32], Livak and Thomas [33] in Cu–Ni–Fe, Enami *et al.* [34] in Ni–Al, Higgins *et al.* [35] in Fe–Be, and Kubo and Wayman in β-CuZn [5]. One example is given in Fig. 6(a1).

It is also interesting to note that the superposition of the mutually perpendicular concentration modulations locally generates a transient microstructure which looks like a 2D square "macrolattice" [arrows in Fig. 2(b2, c2)]. The macrolattice sites are formed by particles of "dark" and "white" phases which appear at nodes of overlaps of the two 1D modulations along [10] and [01] directions, e.g. the "dark" phase particles at intersections of two minimum amplitudes and the "white" phase particles at intersections of two maximum amplitudes. In addition to the "dark" and "white" phases whose compositions are close to the equilibrium compositions, there are "grey" linkages of an intermediate composition between the "dark" and "dark" or "white" and "white" particles. A possibility of such a transient "three-phase" modulated structure has already been predicted from the thermodynamic stability analysis [36]. It was also observed by many investigators using TEM and particularly by de Vos in ALNICO alloys [4].

Later development of this intermediate structure leads to a sandwich-like multi-domain structure consisting of alternating strip-like domains of two equilibrium phases [Fig. 2(d2)]. All domains are well orientated along either [10] or [01] elastically soft directions forming different colonies. A similar structure was obtained by Nishimori and Onnki [37] from a numerical solution to the Cahn–Hilliard equation. The next stage of morphology evolution (e.g. structures from d2 to e2 in Fig. 2) consists of coarsening of both domains and colonies. The coarsening occurs by growth of bigger domains and colonies at the expense of smaller ones. As a result, the average thickness of different domains and average size of colonies increase. The domain coarsening is driven by an interfacial energy reduction while the colony coarsening is driven by a reduction of the part of energy which is proportional to the colony boundary area. Ultimately, the system should reach a stable structure with a single colony of alternating $\{01\}$ domains.

When B^* is assumed to have values between 0 and 2.0, some intermediate structures in between the two cases shown in Fig. 2 are obtained. The larger the value of B^*, the stronger the anisotropy of the structure formed.

4.1.2. Spinodal decomposition in asymmetrical cases. This simulation describes a precipitation in an alloy whose composition, $c = 0.14$, is close to one side of the spinodal line. The aging temperature T^* is again chosen to be 0.08. The representative point on the phase diagram is shown by point "b" in Fig. 1. According to the phase diagram, the volume fraction of the precipitate phase is about 13.8%. Several simulations with the same w_1 and w_2 but different B^* are performed. Some of the results are shown in Fig. 3. In the first row of Fig. 3, where the strain energy parameter B^* is assumed to be zero, randomly oriented concentration waves develop first. An interconnected structure [Fig. 3(a1)] which is similar to that obtained in the symmetrical case is predicted at the initial stage of decomposition. Upon further

aging, however, the connectivity is broken while the two phases grow towards their equilibrium compositions. Instead of an interconnected morphology, isolated circular precipitate particles embedded in the solute-lean dark matrix are formed [Fig. 3(b1–e1)]. These results are different from that predicted by the linear theory [31]. According to [31], connectivity between the two product phases in spinodal decomposition is maintained over a very wide range of volume fraction of the second phase (approximately 15–85%). In our simulations, however, discrete equiaxed particles are obtained even when the volume fraction of the precipitate phase is up to 25%. Therefore, the morphologies developed at later stages of decomposition could be quite different from that formed in the initial stages.

Coarsening of the uniformly distributed equiaxed particles simply follows the LSW mechanism, i.e. larger particles grow and smaller particles shrink to provide an interfacial energy relaxation. As a result, there is a gradual shrinkage of the side-band rings in the diffraction patterns which implies a continuous increase in the mean particle size. The coarsening also results in a wider particle size distribution which is indicated by a transformation of the initially sharp side-bands into diffuse ones.

If finite values of B^* are assumed, totally different morphologies develop. Two examples with $B^* = 1.25$ and $B^* = 1.70$ are shown in the second and third rows of Fig. 3, respectively. In general, the effect of the elastic strain on the initial stage of decomposition, as demonstrated in Fig. 3(a2, a3), is similar to that in the symmetrical case. Fine and diffuse concentration modulations along the elastically soft directions develop first. The larger the strain energy contribution, the stronger the modulation alignment. A noteworthy result of this simulation, however, is the appearance of a regular array of solute-rich "white" equiaxed particles within the solute-lean "dark" matrix in the case of a moderate strain energy contribution ($B^* = 1.25$). The particles are formed at nodes produced by intersections of maxima of the two mutually perpendicular concentration modulations along [10] or [01] directions [Fig. 3(b2)]. The nodes develop into isolated particles by absorbing solute atoms from all connecting linkages. As a result, an array of precipitates which can be best described as a square precipitate macrolattice is formed. The macrolattice generates Laue diffraction maxima with the most intense satellites located at the $\langle 01 \rangle$ soft directions around the Bragg reflection of the atomic lattice. This result is similar to that obtained from a thermodynamic analysis for cubic alloys [16]. Based on the strain energy minimization in a 3D space, a simple cubic precipitate macrolattice was predicted in [16]. However, it should be noted that the precipitate macrolattice obtained here from the kinetic consideration is far from perfect. There is a fairly large amount of macroscopic defects similar to "macrodislocations" and "macrovacancies". The structures shown in Fig. 3(b2–d2) are in excellent agreement with the corresponding electron microscopic image of the macrolattice formed in Fe–Be alloys obtained by Tyapkin *et al.* [2, 3] [see, e.g. Fig. 6(b1)].

As compared to the uniformly distributed particles obtained in the previous case (first row of Fig. 3), the size distribution of this regular array of particles is narrower and its coarsening proceeds discontinuously by two mechanisms different from Ostwald ripening. The first one is a "macrodislocation" climb. For example, the structural evolution from c2 to d2 in Fig. 3 demonstrates disappearance of some particles at the ends of certain rows. The second mechanism is an aggregation of closely located particles. These processes generate "macrovacancies".

The shape of the particles is equiaxed during the early stage of coarsening, but some particles in the same row or column start to aggregate during the later stages forming elongated particles along one of the $\langle 01 \rangle$ soft directions. As a result, a morphology consisting of a mixture of equiaxed and elongated particles is obtained [Fig. 3(e2)].

Increasing B^* has a similar effect on the microstructural development as increasing the "aging" time. The morphological evolution with $B^* = 1.70$ (third row in Fig. 2) shows that elongated particles are formed at an earlier stage of coarsening and the number of elongated particles increases as the "aging" time increases. When t^* reaches 180 [Fig. 3(e3)], almost all the particles exist in the form of $\{01\}$ strips, forming a rough Widmanstätten structure.

If the value of B^* is much smaller than 1.25 e.g. about 0.7, the equiaxed particles formed are not well aligned along the $\langle 01 \rangle$ directions. On the other hand, if B^* is very large, e.g. >2.0, the intermediate macrolattice structure does not appear. The system directly decomposes into a structure consisting of individual strip-like particles with $\{01\}$ habits embedded in the matrix.

All these results indicate that the precipitate macrolattice appears only as a temporal morphological state during a phase transformation. The appearance of such a morphological state depends on both the lattice mismatch characterized by B^* and the aging time.

4.2. Morphological evolution during decomposition above spinodal

The cases considered above demonstrate that if the strain effect is taken into account, quasi-periodic concentration modulations aligned along the elastically soft directions always appear in the beginning of a spinodal decomposition. Experimental observations, however, show that some modulated structures are formed from initially randomly distributed precipitates as well [8–10]. Such a morphological evolution most likely follows a nucleation and growth mechanism which is operative above the spinodal line. Therefore, it is interesting to investigate

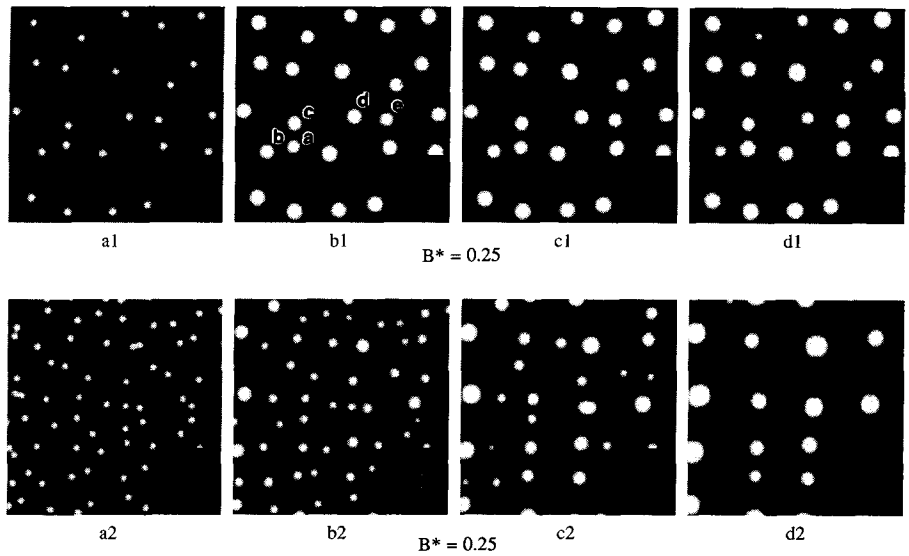

Fig. 4. Rearrangement of initially randomly distributed particles formed by a nucleation and growth mechanism during strain-induced growth and coarsening processes. Alloy composition and "aging" temperature are presented by point "c" in Fig. 1. (a1)–(d1) and (a2)–(d2) correspond to $t^* = 2$, 200, 500 and 1000. 1 and 2 here designate differences in density of nuclei.

isothermal "aging" of an alloy in this part of the phase diagram. This is the case when an alloy with composition $c = 0.12$ is quenched to a point "c" shown in the phase diagram (Fig. 1). Since our kinetic equations always drive a system towards states with lower free energies, it cannot describe an activation process such as nucleation which requires overcoming an energy barrier. Therefore, nuclei have to be introduced artificially. This is done by randomly placing nuclei into a homogeneous disordered solution. The size of the nuclei has been chosen to be larger than the critical size.

Evolutions of the initially randomly distributed small particles under the influence of a moderate elastic strain effect are demonstrated in Fig. 4. Two different cases are presented. In the first case where a lower density of nuclei is assumed, an interesting multi-particle effect, i.e. selective growth and translational motion of particles during their growth and coarsening processes is observed. It is demonstrated in the first row of Fig. 4. In order to see clearly this effect, we superimposed Fig. 4 (d1) onto (a1). The result is presented in Fig. 5. It is shown that the initially randomly distributed particles have a tendency to grow and migrate along certain directions to form regular arrays along the $\langle 01 \rangle$ directions. As a result, a rough precipitate macrolattice is formed. It is reflected by a gradual appearance of satellites in the diffraction patterns shifted from the Bragg reflection along the $\langle 10 \rangle$ directions. The directions of the growth and translational motion of particles are determined by their relative displacements from the macrolattice sites.

In addition to the selective growth and translational motion, the entire coarsening process of the particles is quite different from Ostwald ripening. Examining the microstructural development from (b1) to (d1) shown in Fig. 4, one may see that the coarsening is determined by the relative position of a particle rather than by its size. For example, if we concentrate on the three particles marked a, b and c, or the two particles marked d and e in those pictures, it can be readily seen that the initially smaller particles a and e grow larger at the expense of the initially larger particles b, c and d. Such a coarsening process is just opposite to that of Ostwald ripening. It is unique and is caused by the strain energy relaxation. We call this process the strain-induced reverse coarsening. A possibility of such a reverse coarsening

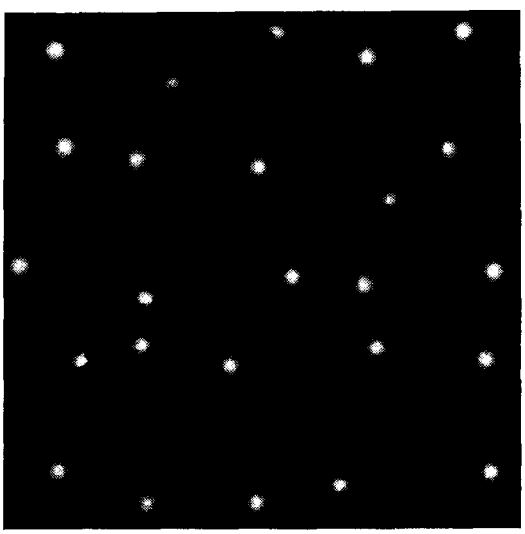

Fig. 5. Superimposition of (a1) and (d1) of Fig. 4 showing the selective growth and translational motion of particles during strain-induced growth and coarsening in a multi-particle system.

behavior has been predicted by Khachaturyan and Shatalov [13] from the strain energy consideration. But this prediction is not quite convincing since it was based on thermodynamic arguments only. Johnson *et al.* [23] obtained the reverse coarsening effect by considering diffusion kinetics, but they analyzed only a two-particle system. Indeed, as shown in Fig. 5, the strain-induced reverse coarsening in a multi-particle system could be substantially different from that in a two particle system. It is directed to restore the periodical particle arrangement.

When a higher density of nuclei is assumed, a more regular precipitate macrolattice is formed by selective growth and selective coarsening processes [Fig. 4(a2–d2)]. Here by selective growth we mean that the particles which sit at or close to the "macrolattice sites" grow much faster than those who are located at the "interstitial sites". The selective coarsening means that all "interstitial" particles disappeared during the coarsening process. The microstructures shown in Fig. 4 are in excellent agreement with the observations by Tyapkin *et al.* in Ni–Cu–Si alloys [9] and in Fe–Mn–Al–C alloys [10]. One example is given in Fig. 6(c1).

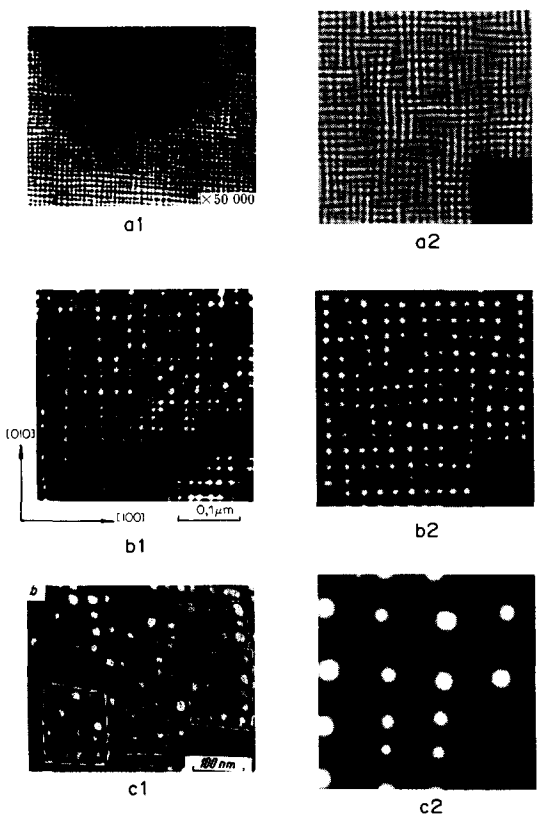

Fig. 6. Comparison between experimental observations [(a1)–(c1)] and computer simulation results [(a2)–(c2)], (a1) basket-weave structure formed in ALNICO alloy, foil orientation (001) (from [4]), (b1) precipitate macrolattice formed in Fe–Be alloy, foil orientation (001) (from [3], Engl. Transl.), (c1) formation of regular array of $\gamma'(L1_2)$ particles from originally randomly distributed precipitates in Ni–Cu–Si alloy, foil orientation (001) (from [8], Engl. Transl.); (a2) copy of Fig. 2(b2), (b2) copy of Fig. 3(d2), (c2) copy of Fig. 4(d2).

Figure 7 shows a temporal morphological evolution in a case that involves both nucleation and growth and spinodal mechanisms. This is realized by

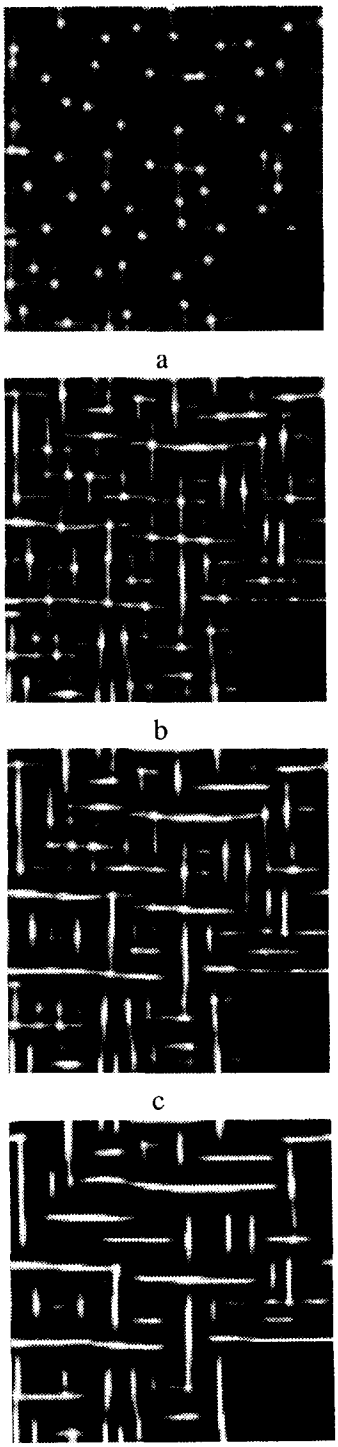

Fig. 7. Temporal morphological evoluation in an alloy of $B^* = 2.0$ which undergoes a two step "aging treatment" described by point "d" and "e" in Fig. 1, (a)–(d) correspond to $t^* = 2$, 10, 50 and 100.

a two step "aging treatment". An alloy with composition $c = 0.14$ and $B^* = 2.0$ is first "aged" at a higher temperature above the spinodal line (point d in Fig. 1). The nucleation process of this alloy is simulated by artificially introducing randomly distributed nuclei. After a certain period of time, the alloy is "aged" at a lower temperature well below the spinodal line (point e). As shown in Fig. 7(a), a highly anisotropic growth is obtained. The nuclei grow only along the two elastically soft directions. The diffusion fields around each particle have a four-fold symmetry, i.e. solute atoms around the particle diffuse from all the other directions towards the [10] and [01] soft directions. As a result, linkages between growing precipitates occur along the soft directions, resulting in formation of individual strip-like particles with {01} habits.

4.3. Morphological development dominated by elastic strain energy and formation of GP zones

As has been demonstrated above, two-phase morphologies developed in precipitation reactions are determined by a balance between the strain-induced infinite radius interaction and the "chemical" finite radius interaction. The effect of the finite radius interaction on morphology in macroscopic terms is described by the interfacial energy. A limit case when the strain energy contribution is zero and the morphological evolution is totally controlled by the interfacial energy has been investigated above. It would be interesting to investigate the other extreme case when the morphological development is primarily controlled by the strain energy and the interfacial energy contribution is almost negligible. In the following simulation we choose a dilute solid solution with $c = 0.05$ (point f in Fig. 1) in which the reduced strain energy parameter B^* reaches an extremely high value 7.0.

Figure 8 illustrates the computer simulation results of spinodal decomposition in such a system driven primarily by the strain energy relaxation. At the initial stage of decomposition [Fig. 8(a)], ⟨01⟩ satellites appear in the diffraction pattern before any visible phase separation occurs. In order to understand the origin of these satellites, we magnified the concentration inhomogeneities in Fig. 8(a). As shown in Fig. 8(b), very diffused concentration modulations are resolved. As aging proceeds, solute-rich "white" phase starts to precipitate as very thin strips along the elastically soft directions. What is surprising is that all the precipitates have a thickness of one atomic layer and the concentration profiles are step functions. This is particularly reflected by rod-like streaks along the ⟨01⟩ directions which appear in the diffraction patterns. There is no coarsening (thickening) during the entire "aging" process. These results could be used for explaining the origin of the {001} GP zones formed in Al–Cu and Cu–Be alloys characterized by extremely high crystal lattice mismatch ($da/adc \sim 10\%$). As is known, the GP zones in these materials are Cu rich and Be rich single atomic layers [38–40].

If the atomic size mismatch is not so high and the finite radius interaction plays a greater role, multi-atomic layer strip-like precipitates that may be referred to as multi-layer GP zones are obtained. They are formed by either a direct precipitation or a subsequent coarsening (thickening) from the initially precipitated strip particles of one or two atomic layers. The thickening follows a ledge-growth mechanism as observed by Garg and Howe in Al–Cu–Mg–Ag alloy [41], i.e. by nucleation and lateral growth of ledges parallel to the {01} interface. The equilibrium number of atomic layers depends on the balance between the finite radius interaction energy and the infinite radius strain-induced interaction energy at the aging temperature. Formations of the multi-layer GP zones in both Al–Cu and Cu–Be alloys have recently been reviewed by Koo and Cohen [42].

4.4. Shape evolution of a single coherent new phase particle during strain-induced coarsening

Recent TEM studies [6, 7] have revealed a very interesting instability which occurs in the phase transformation of Ni–Al alloys. It is observed that γ' phase first precipitates as cuboidal particles. Then during the coarsening process, some large particles resist further coarsening and split into doublets of parallel plates [6] or octets of smaller cubes [7]. Typical TEM pictures showing this process are given in Fig. 9(a). The thermodynamic analysis of this phenomenon [6, 43] suggests that splitting of the large cuboidal γ' particles is caused by a relaxation of the transformation-induced elastic strain. However, kinetics of the splitting process is not well understood. The following simulation is an attempt to show kinetically how a particle splits, e.g. where the instability starts and how it develops.

We start the simulation with a single circular particle which has an equilibrium composition, $c_\beta = 0.982$ (corresponding to an aging temperature $T^* = 0.12$), and a radius, $r = 25a$, where a is the lattice parameter. The particle is embedded in a $128a \times 128a$ matrix with an equilibrium composition $c_\alpha = 0.018$. The representative point "g" on the phase diagram (Fig. 1) is just above the spinodal line. The coarsening of this particle is then simulated by its diffusional relaxation at different values of the reduced strain energy parameter B^*. According to the thermodynamic analysis [43], the equilibrium shape of a coherent particle at a given volume V is determined by the strain energy to interfacial energy ratio

$$K = \frac{E_{el}}{E_s} \sim \frac{BV}{\gamma S} \tag{18}$$

where γ is the specific interfacial energy and S is the total interfacial area. The parameter, K, is a scaling factor charaterizing the combined effects of

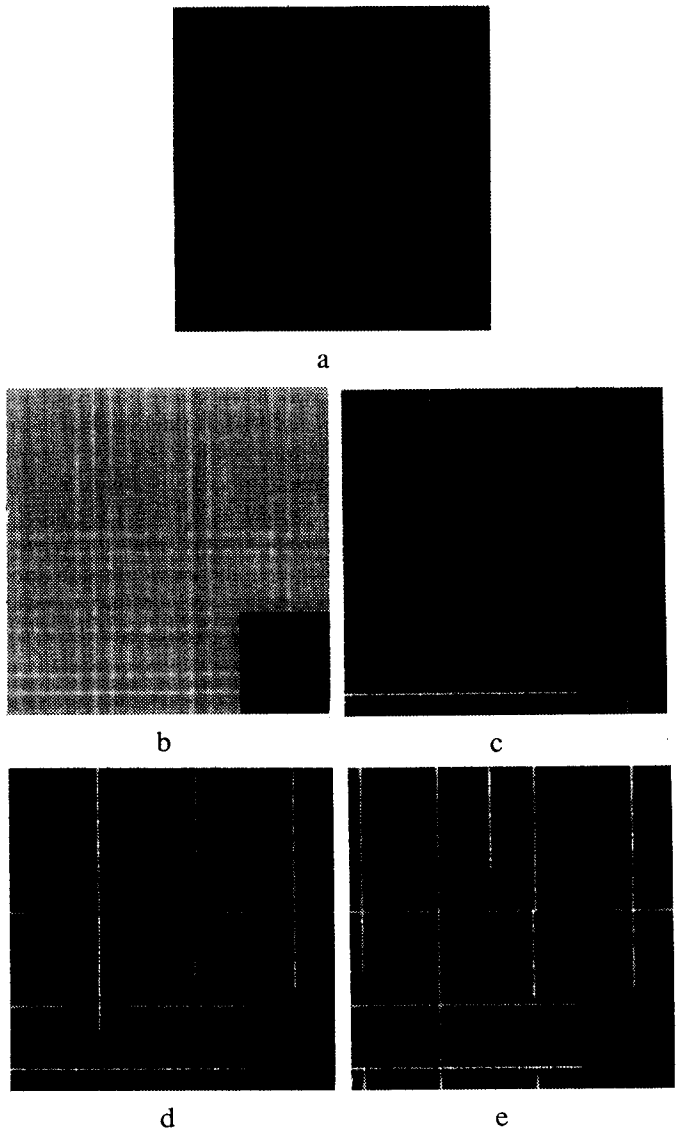

Fig. 8. Morphological evolution in a dilute solid solution during decomposition driven primarily by strain energy relaxation. The thickness of the "white" precipitates is one atomic layer. (a) and (b) represent the same morphology developed at $t^* = 170$ but with concentration inhomogeneity magnified in (b) to resolve the satellites appeared in the diffraction pattern. (c)–(e) correspond to $t^* = 190, 200, 500$.

interfacial tension and elastic strain. It shows that an increase in the strain energy parameter, B, may produce the same effect on the equilibrium shape as an increase in the precipitate volume upon coarsening. Therefore the sequences of shape relaxation of a coherent particle with respect to an increase in B actually simulate effects which should be observed due to an increase in the particle volume during the coarsening process at a fixed value of B. This scaling concept dramatically simplifies the numerical calculations.

The assumed initial circular shape actually represents the initial stage of a coarsening process where small and sparsely distributed particles are usually obtained. Shapes of these particles are primarily determined by the interfacial energy minimization. Being volume dependent, however, the strain energy contribution increases considerably with coarsening and eventually dominates over the interfacial energy during the later stages when the surface to volume ratio is small. A strain-induced shape transformation of the spheroidal particles should then be expected.

The simulated results are shown in Fig. 10. In the first row of Fig. 10, the dependence of equilibrium shapes of the particle on B^* (which characterizes the strain energy contribution at a certain volume) is illustrated. The initial value of B^* is assumed to be zero. In this case the diffusional relaxation does not result in shape changes [Fig. 10(a)]. The only change is a transformation of the initially sharp interface into a diffuse one. As B^* increases, there is a continuous

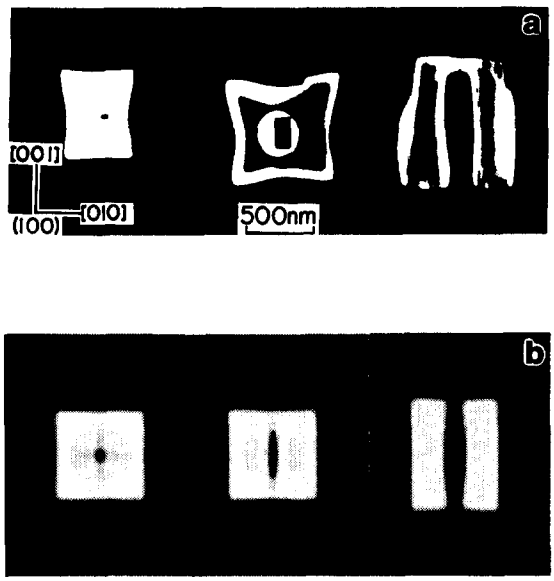

Fig. 9. (a) A TEM dark field image of splitting sequence of γ' particles in Ni–12 at.% Al single crystal (from [6]), (b) computer simulation results [copies of (g), (h) and (j) of Fig. 10].

change in the curvature of the particle interface, which gradually transforms the circular particle into a square with {10} interfaces [Fig. 10(b–d)]. At each increment of B^*, the system is "aged" for a time duration which is long enough to establish an equilibrium configuration. The squares formed at larger values of B^* are more pronounced, having sharper corners and slightly concave edges. The concentration profiles inside the particle and around it are homogeneous for small values of B^* but inhomogeneous for greater values. For example, concentration inhomogeneities are developed both inside and outside the particle at $B^* = 2.2$ [Fig. 10(d)].

With a further increase of B^*, the square configuration shown in Fig. 10(d) becomes unstable. Development of the instability and formation of the plate doublet at $B^* = 2.3$ are presented in the second and third rows of Fig. 10. When B^* reaches the value of 2.3, the concentration inhomogeneity inside the particle is so high that a matrix phase (dark) particle reversely precipitates at the center of the square

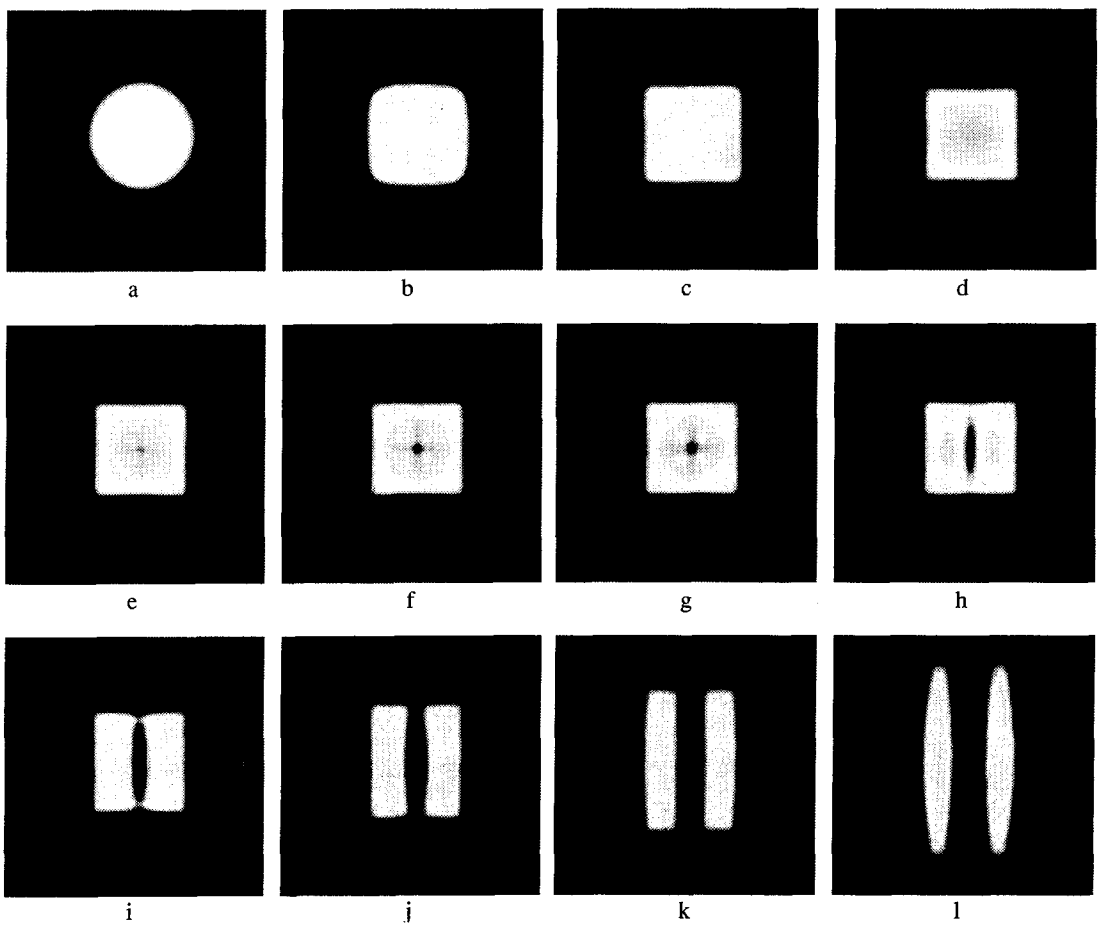

Fig. 10. Simulated sequences of shape relaxation and splitting of a coherent particle during its strain-induced coarsening. Pictures shown in the first row represents equilibrium shapes of the particle at different reduced strain energy parameters, (a)–(d) correspond to $B^* = 0.0, 0.2, 0.9, 2.2$. Pictures shown in the second and third rows represent splitting sequences of the particle at $B^* = 2.3$, (e)–(l) correspond to $t^* = 200, 260, 300, 400, 650, 1000, 1500, 2000$.

particle. This matrix phase particle grows anisotropically along the two elastically soft directions in a similar fashion as that shown in Fig. 7(a). The four-fold symmetry growth demonstrates a tendency to split the square into a quartet of smaller squares with the same {01} interfaces. However, the four-fold symmetry of the anisotropic growth is broken and the growth along one of the ⟨10⟩ direction prevails. It results in the appearance of an ellipse-like particle of the matrix phase in the center of the square precipitate [see Fig. 10(h)]. Further growth of the elliptical particle along [01] direction splits the square into a rectangular doublet with {01} interfaces. These configurations are shown in Fig. 10(e–l). As soon as the square is split into the doublet, the concentration inhomogeneity inside the precipitates disappears. When the doublet approaches its equilibrium configuration, the concentration inhomogeneity within the matrix phase disappears as well.

5. DISCUSSION

When the coherent elastic strain effect is taken into account, a wide variety of morphological states can be developed at different stages of a precipitation reaction in systems with a miscibility gap. To study the strain-induced morphological transformation in such systems, the microscopic kinetic model employed in this paper has been proved to have several obvious advantages over the conventional methods. First, it does not need any *a priori* assumptions about the possible morphologies that develop in a precipitation reaction such as shapes, habits, concentration profiles and spatial distributions of the precipitate particles. All the structural changes are described by a relaxation of the nonequilibrium occupation probability function, $n(\mathbf{r}, t)$. Second, the model is quite general since it simultaneously describes several kinetic processes involved in a precipitation reaction such as ordering (if the precipitate phase is an ordered intermetallic), decomposition, growth and coarsening. These processes are usually treated using different mathematical formulations and models. Finally, it allows us to investigate all the intermediate morphological states that appear during the development of a stable microstructure. The main limitation of this approach is that it cannot describe activation processes and particularly nucleation. Therefore, artificial nuclei have to be introduced to describe temporal evolution of a metastable state.

The simulations performed in the framework of the adopted kinetic model demonstrate that the transformation-induced elastic strain results in certain spatial precipitate patterns in a multi-particle system irrespective of the decomposition mechanisms. Typical examples are the formation of basket weave structures, sandwich-like multi-domain structures, precipitate macrolattices and GP zones. These results cannot be obtained by using the classical thermodynamic approaches to phase transformations based on consideration of the finite radius interactions only. The pattern formation is caused by the long-range interactions between the strain fields generated by different concentration heterogeneities. These long-range interactions tend to arrange or rearrange the new phase particles in such a way that the strain fields from individual particles are nullified to provide a strain relaxation. The shapes of the individual particles forming the patterns are, however, determined by both the strain and interfacial energies. Therefore, it is actually the interplay between the elastic and interfacial energies that determines the entire characteristics of a microstructure. According to the balance between these two energies, morphological developments may be roughly divided into three cases in which the development is controlled by (i) relaxations of interfacial energy, (ii) both interfacial and strain energies and (iii) strain energy.

(i) In the first case, microstructures with an isotropic characteristic are formed and the morphological development simply follows the LSW mechanism to provide a relaxation of the assumed isotropic interfacial energy (see, e.g. the pictures shown in Figs 2 and 3 for $B^* = 0.0$). When the two product phases have approximately the same volume fraction as in the symmetrical spinodal decomposition, the two phases are highly interconnected. But if the volume fraction of one phase is considerably different from the other, randomly distributed discrete equiaxed particles are formed.

(ii) Typical morphological development in the second case, where both the strain energy and interfacial energy contributions are significant, is formation of the precipitate macrolattices in both asymmetrical spinodal decomposition and nucleation and growth processes. These results should not be surprising if we follow the energy analysis proposed by Khachaturyan and Airapetyan [16]. According to [16], if a new phase precipitates as equiaxed particles coherently embedded in a matrix, a minimum energy state is reached when the particles form one of the 14 Bravais lattices. In the asymmetrical cases, structures developed in both processes, spinodal decomposition and nucleation and growth studied above, have a common characteristic, i.e. a minor phase forms discrete particles embedded in a major phase matrix. These particles should arrange or rearrange themselves to form a macrolattice, providing a strain energy relaxation. However, it should be noted that in order to form a macrolattice, the strain energy cannot be too large since shapes of the discrete particles forming the lattice are determined by competition between the interfacial and strain energies. As demonstrated in our computer simulation (Fig. 3), the macrolattice exists only in alloys which have a moderate degree of atomic size mismatch and only temporarily at certain stages of decomposition when the strain energy effect is balanced by the interfacial energy. Therefore in order to form a precipitate macrolattice, the strain energy should be small

enough to preserve the equiaxed particle shape minimizing the isotropic interfacial energy, but it should be sufficient to provide a regular spatial distribution of precipitates. This is a general condition applied irrespective of the decomposition mechanisms, although the kinetic evolution paths may be different in different cases. For example, in spinodal decomposition, the macrolattice is formed by a superposition of the $\langle 01 \rangle$ concentration waves developed in the initial stage of decomposition. The position of the particles are predetermined by intersections of the maximum amplitudes of the two kinds of concentration waves. In the case of nucleation and growth, the macrolattice is formed by the strain-induced selective growth, reverse coarsening and translational motion of the initially randomly distributed particles.

Several interesting kinetic phenomena, such as the selective and anisotropic growth, particle translational motion, "macrodislocation" climb coarsening and reverse coarsening are revealed during the strain-induced growth and coarsening of the precipitate macrolattice. These phenomena cannot be interpreted in terms of the LSW coarsening theory. A significant particle translational motion is observed in the rearrangement of the initially randomly distributed particles. According to [1], this translational motion is caused by a strain-induced variation of chemical potential along the precipitate boundaries. Driven by this chemical potential inhomogeneity, solute atoms diffuse from one side of the particle to the other side to equalize the chemical potential. This phenomenon was discussed in [44]. For a two particles system, the kinetics of translational motion caused by the elastic strain was studied by Johnson *et al.* [23]. They obtained a motion of two particles towards one another when they are aligned along the elastically soft direction.

To the best of our knowledge, the present study is the first attempt to investigate such kinetics for a multi-particle system. Figure 5 demonstrates that particles aligned along the soft directions may even move away from each other during the strain-induced coarsening process. The directions of motion of particles in a multi-particle system are actually dominated by their tendency to form a "macrolattice". In general, the growth and coarsening behaviors of the particles forming the precipitate macrolattice are determined by their displacements from the more stable macrolattice sites. The macrolattice sites are determined by thermodynamic factors characterizing the competition between the strain and interfacial energies and kinetic factors controlling the diffusion distance as well.

(iii) The origin of Guinier–Preston zones in Al–Cu and Cu–Be dilute alloys, in spite of more than four decades of research, is still a controversial issue in physical metallurgy. GP zones in these systems are single $\{001\}$ planes enriched by Cu or Be atoms which are imbedded in the Al and Cu f.c.c. matrix, respectively. Our computer simulation seems to suggest an explanation for this phenomenon. When the strain energy makes a dominant contribution over the finite radius interaction energy, the decomposition leads to an appearance of single-layer $\{01\}$ precipitates. According to their structural characteristics, these single atomic layer precipitates are just GP zones [Fig. 8(c–e)]. This theoretical prediction makes Al–Cu and Cu–Be systems prime candidates for alloys where GP zones could be expected. Indeed, these systems have negative elastic anisotropy, which provides the $\{001\}$ orientations of GP zones perpendicular to the $\langle 001 \rangle$ elastically soft directions. But what is most important is that these systems belong to a group of very rare alloys whose crystal lattice mismatch, characterized by the crystal lattice expansion coefficient da/adc, is extremely high, e.g. larger than 0.1. This value approaches the theoretical limit of a solid solution, $da/adc \approx 0.15$, above which no solubility can exist. With the value $da/adc \sim 0.1$, the strain energy exceeds (by orders of magnitude) the typical mixing energies of substitutional alloys. Under this condition the thermodynamic behavior of the system and particularly its miscibility gap is determined by the strain-induced interaction only. Increasing the contribution of the finite-radius interaction results in thickening of the GP zones to two or more number of atomic layers. Therefore, our results show that GP zone morphology occurs as a result of the usual decomposition under the condition that the strain-induced interaction far exceeds all other interchange interactions. Then GP zones are just thin platelike precipitates whose thickness reaches the least limit permitted by the crytallography, one atomic layer.

Another interesting morphology developed, when the morphological evolution is controlled by the strain energy, is the so-called basket-weave structure [Fig. 2(a2–c2)]. It is obtained during a symmetrical spinodal decomposition where the volume fractions of the two product phases are equal. The origin of this structure is a superposition of concentration waves developed along the two elastically soft directions in the early stage of decomposition. The basket-weave structure is unstable with respect to transformation into sandwich-like multi-domain structures [Figs 2(d2) and (e2)].

The interplay between the interfacial and strain energies is also clearly demonstrated by the shape evolution of a single circular coherent particle during its coarsening process. The coarsening provides a consequent realization of the three cases discussed above. For example, the process can be divided into three stages, i.e. initial, intermediate and final stages corresponding to the first, second and third cases, respectively. During the initial stage, the particle is very small and the interfacial energy contribution is dominant. In this case the particle shape is primarily controlled by the interfacial energy relaxation. As a result, the particle maintains a circular shape as demonstrated in Fig. 10(a). This stage may be

described by the LSW theory. According to the strain energy-to-interfacial energy ratio (18), growth of the particle (increase of its volume V) increases the strain energy contribution. It becomes comparable with the interfacial energy at the intermediate stage of coarsening. During this stage, a significant shape change from a circle to a square gradually occurs [see Fig. 10(b–d)]. Such a coarsening process, which is controlled by the balance between the interfacial energy and strain energy relaxations, cannot be described by the LSW theory. In the third stage of coarsening, the precipitate volume increases to such an extent that the strain energy contribution becomes dominant and the coarsening process reverses. The reverse coarsening is manifested by splitting the square particle into doublets, which is just opposite to what is traditionally expected.

Splitting from a square to a doublet starts by reverse precipitation of a matrix phase particle in the center of the square [Fig. 10(e–h)]. Since our computer simulation cannot describe a nucleation process, as mentioned before, the shape transformation from the square to the doublets really occurs with a hysteresis, i.e. at a substantially larger volume compared to those from thermodynamic calculations [24]. It indicates a metastable character of the "overgrown" square. The absolute instability of the metastable square with respect to infinitesimal concentration fluctuations results in a concentration inhomogeneity in the center of the square. It is in equilibrium at each given particle size. The infinitesimal fluctuations appear in our computer simulation automatically due to a finite accuracy of the computer computations. The inhomogeneity keeps growing until the square particle is split into a doublet. These simulation results are in surprisingly good agreement with the electron microscopic observations (see, e.g. Fig. 9). The electron microscopic images in the (001) plane [Fig. 9(a)] clearly demonstrate splitting of the cuboidal γ' (Ni_3Al) precipitates in Ni–Al alloy into plate doublets by nucleation of a "hole" in the center of a particle. This is also in agreement with the computer simulation based on the elementary particle approximation [22]. Since the overgrowth square is metastable in a certain size range, the splitting within this range may occur by nucleation of a matrix phase particle within the square.

It should be mentioned that the situation may be different in a 3D case. For example, we could speculate that the instability could also start in the center of cube faces. The electron microscopic observations by Kaufman *et al.* [7] show that such an interpretation is also possible. The extension of this 2D simulation to 3D will not pose any additional difficulties except longer computation time. Corresponding work on 3D simulation is under way.

Some preliminary results on the shape evolution of a coherent particle and its splitting were published in our work [24]. This phenomenon has also been recently investigated by Voorhees *et al.* [45] who used a continuum approximation. These authors obtained a shape transition from a circle to a square with rounded angles. But they could not predict splitting since they postulated homogeneous equilibrium composition within the particle.

In the present work, a homogeneous modulus approximation is used. As has been shown by Voorhees and Johnson for two spherical particle coarsening [46, 47] and by Kawasaki and Enomoto for multiple sphere particle coarsening [48] in elastically isotropic systems, and more recently by Onuki and Nishimori in their 2D computer simulations of spinodal decomposition based on a time-dependent Ginzburg–Landau model [49], the modulus mismatch between the two phases has a substantial effect on the coarsening kinetics.

6. CONCLUSION

The kinetics of isostructural decompositions in the presence of elastic strain was studied using a computer simulation technique based on the nonlinear microscopic diffusion theory. Results show that the transformation-induced elastic strain drastically affects the two-phase morphology during both spinodal decomposition and nucleation and growth processes. Controlled by the interplay between the interfacial energy and the strain energy, various types of coherent two-phase morphologies as well as different kinetic phenomena are predicted.

1. Below the spinodal, well-defined modulated structures start to form during the incipient stage of decomposition. The structure is highly anisotropic if its growth is dominated by the strain energy. The larger the crystal lattice mismatch, the more pronounced the structural anisotropy. The well known basket-weave structures are obtained as an intermediate morphological state during the development of sandwich-like multi-domain structures in a symmetrical spinodal decomposition. It is formed by a superposition of the concentration waves along the [10] and [01] "soft" directions. In the asymmetrical case, spinodal decomposition results in a quasi-periodic precipitate macrolattice if the strain energy contribution is balanced by the interfacial energy. The superposition of the concentration modulations predetermines the occurrence of the macrolattice in the later stages of aging. The coarsening of this structure follows a "macrodislocation climb" mechanism.

2. The computer simulation allows us to predict the formation of GP zones. Single-layer GP zones are formed in the extreme case of a very high crystal lattice mismatch. When the finite radius chemical interaction is strong and cannot be ignored, multilayer GP zones could be expected. These results suggest that the GP zone formation is a particular case of decomposition within a miscibility gap given a condition that the strain-induced interaction dominates the thermodynamics.

3. Above the spinodal, a rearrangement of initially randomly distributed particles due to the strain-induced selective growth, particle translational motion and reverse coarsening is predicted. The rearrangement also results in a rough precipitate macrolattice in the case of a moderate crystal lattice mismatch.

4. A shape transformation of a single coherent particle during strain-induced coarsening caused by a competition between the elastic and interfacial energies is obtained. Specifically for this 2D model system, a circular precipitate shape was found to transform to a square and then to a plate doublet. The transformation from the square to the doublet starts by reverse precipitation of a matrix phase particle at the center of the square, while the transformation from the circle to the square is continuous.

All these results seem to be in good agreement with experimental observations, indicating that this 2D model describes fairly well the most essential features of the strain-induced microstructural developments in alloys with a miscibility gap. Regardless of its oversimplification, it can be efficiently used in many cases for understanding, interpreting, and predicting structural evolution in real alloys.

Acknowledgements—The authors gratefully acknowledge the support by National Science Foundation under grant No. NSF-DMR-91-23167. The simulation was performed on Cray-YMP at the Pittsburgh Supercomputing Center. We are grateful to S. Ganesh for his comments on the manuscript.

REFERENCES

1. A. G. Khachaturyan, *Theory of Structural Transformations in Solids*. Wiley, New York (1983).
2. Yu. D. Tyapkin, N. T. Travina and T. V. Yevtushenko, *Fizika Metall.* **45,** 613 (1978); *Physics Metals Metallogr.* (Engl. Transl.) **45,** 140 (1978).
3. Yu. D. Tyapkin, Ye. I. Maliyenko, I. V. Gongadze and S. M. Komirov, *Fizika Metall.* **68,** 755 (1989); *Physics Metals Metallogr.* (Engl. Transl.) **68,** 125 (1989).
4. K. J. de Vos, thesis (1966).
5. H. Kubo and C. M. Wayman, *Metall. Trans.* **10A,** 633 (1979).
6. T. Miyazaki, H. Imamura and T. Kozakai, *Mater. Sci. Engng* **54,** 9 (1982).
7. M. J. Kaufman, P. W. Woorhees, W. C. Johnson and F. S. Biancaniello, *Metall. Trans.* **20A,** 2171 (1989).
8. A. Ardell and R. B. Nicholson, *Acta metall.* **14,** 1295 (1966).
9. Yu. D. Tyapkin, I. V. Gongadze and Ye. I. Maliyenko, *Fizika Metall.* **66,** 589 (1988); *Physics Metals Metallogr.* (Engl. Transl.) **66,** 160 (1988).
10. Yu. D. Tyapkin, Ye. I. Maliyenko, I. V. Gongadze, I. S. Kalashnikov and S. M. Komarov, *Fizika Metall.* **68,** 540 (1989); *Physics Metals Metallogr.* (Engl. Transl.) **68,** 121 (1989).
11. J. W. Cahn, *Acta metall.* **9,** 795 (1961); **10,** 179 (1962).
12. A. G. Khachaturyan, *Soviet Phys. solid St.* **8,** 2163 (1967).
13. A. G. Khachaturyan and G. A. Shatalov, *Soviet Phys. solid St.* **11,** 118 (1969).
14. J. K. Lee, D. M. Barnett and H. I. Aronson, *Metall. Trans.* **8A,** 963 (1977).
15. A. G. Khachaturyan, *Physica status solidi* **35,** 119 (1969); *Soviet Phys. JETP* **31,** 98 (1970).
16. A. G. Khachaturyan and V. M. Airapetyan, *Physica status solidi* (a) **26,** 61 (1974).
17. V. Perkovic, C. R. Purdy and L. M. Brown, *Acta metall.* **27,** 1075 (1979).
18. Ye. I. Maliyenko and Yu. D. Tyapkin, *Fizika Metall.* **57,** 942 (1984).
19. A. G. Khachaturyan and G. A. Shatalov, *Soviet Phys. JETP* **29,** 557 (1969).
20. T. Miyazaki, T. Kozakai and S. Mizuno, *Trans. Japan Inst. Metals* **24,** 799 (1983).
21. S. Wen, J. W. Morris and A. G. Khachaturyan, *Proc. Int. Symp. on Modulated Structures*, Kona, Hawaii, pp. 168–172 (1979); *Metall. Trans.* **12A,** 581 (1981).
22. M. T. McCormack, A. G. Khachaturyan and J. W. Morris, *Acta metall. mater.* **40,** 325 (1992).
23. W. C. Johnson, T. A. Abinandanan and P. W. Voorhees, *Acta metall. mater.* **38,** 1349 (1990).
24. Y. Wang, L. Q. Chen and A. G. Khachaturyan, *Scripta metall. mater.* **25,** 1387 (1991); **25,** 1969 (1991).
25. A. G. Khachaturyan, *Soviet Phys. solid St.* **9,** 2040 (1968).
26. L. Q. Chen and A. G. Khachaturyan, *Scripta metall. mater.* **25,** 61 (1991); **25,** 67 (1991).
27. L. Q. Chen and A. G. Khachaturyan, *Acta metall. mater.* **39,** 2533 (1991).
28. S. M. Allen and J. W. Cahn, *Acta metall.* **24,** 425 (1976).
29. L. Q. Chen, Y. Wang and A. G. Khachaturyan, *Phil. Mag. Lett.* **64,** 241 (1991).
30. V. G. Vaks, A. J. Larkin and C. A. Pikin, *Zh. eksp. teor. Fiz (JETP)* **51,** 361 (1966) (in Russian).
31. J. W. Cahn, *J. chem. Phys.* **42,** 93 (1965).
32. E. P. Butler and G. Thomas, *Acta metall.* **18,** 347 (1970).
33. B. J. Livak and G. Thomas, *Acta metall.* **19,** 497 (1971).
34. K. Enami, J. Hasunuma, A. Nagasawa and S. Nenno, *Scripta metall.* **10,** 879 (1976).
35. J. Higgins, R. B. Nicholson and P. Wilkers, *Acta metall.* **22,** 201 (1974).
36. A. G. Khachaturyan, *I.E.E.E. Trans.* **MAG-6,** 233 (1970).
37. H. Nishimori and A. Onuki, *Phys. Rev. B* **42,** 980 (1990).
38. A. Guinier, *Nature* **142,** 569 (1938).
39. G. D. Preston, *Nature* **142,** 570 (1938).
40. A. Guinier and P. Jaquet, *Rev. Metall.* **16,** 1 (1944)
41. A. Garg and J. M. Howe, *Acta metall.* **39,** 1925 (1991).
42. Y. M. Koo and J. B. Cohen, *Acta metall.* **37,** 1295 (1989).
43. A. G. Khachaturyan, S. V. Semenovskaya and J. W. Morris, *Acta metall.* **36,** 1563 (1988).
44. Ya, Geguzcn and M. A. Krivoglaz, *Migration of Macroscopic Inclusions in Solids*. Consultants Bureau, New York (1973).
45. P. W. Voorhees, G. B. Mcfadden and W. C. Johnson, to be published.
46. P. W. Voorhees and W. C. Johnson, *Phys. Rev. Lett.* **61,** 2225 (1988).
47. W. C. Johnson, P. W. Voorhees and D. E. Zupon, *Metall. Trans.* **20A,** 1175 (1989).
48. K. Kawasaki and Y. Enomoto, *Physica A* **150,** 463 (1988).
49. H. Nishimori and A. Onuki, *J. Phys. Soc. Jap.* **60,** 1208 (1991); *Phys. Rev. B* **43,** 13649 (1991).